

The milliarcsecond-scale jet in the quasar J1625+4134

D. R. Jiang^{1,2}, J. F. Zhou^{1,2}, X. Y. Hong^{1,2}, L. I. Gurvits³, Z.-Q. Shen⁴,

and

Y. J. Chen^{1,2}

ABSTRACT

We present Very Long Baseline Array (VLBA) observations of the radio source J1625+4134 at 22 and 15 GHz and analyze them in concurrence with other existing VLBI data on this source. The high resolution images at 15 and 22 GHz show a short and bending jet which has about 270° difference in position angle with the northern jet detected at lower frequencies. The new high resolution data, combined with the data available in the literature, allow us to estimate the spectral index of the components and identify one of the compact components as the VLBI core based on its flat spectrum between 5 and 22 GHz. Relative to this core component, the jet appears to be bi-directional. The proper motion measurement of the component C2 and the estimate of the Doppler boosting factor suggest that the orientation of the jet is close to the line of sight. The projection effect of an intrinsically sharply bending jet within a few mas from the core or the erratic change in the nozzle direction of the jet may account for the uncommon bi-directional structure of the jet in J1625+4134.

Subject headings: galaxies: active – galaxies: nuclei – galaxies: jets – quasars: individual: J1625+4134

1. INTRODUCTION

The radio source J1625+4134 (1624+416; 4C41.32) was identified as a quasar at the redshift of $z = 2.55$ (Pearson & Readhead 1988; Hewitt & Burbidge 1993). It has a 22^m

¹Shanghai Astronomical Observatory, Chinese Academy of Sciences, Shanghai 200030, China

²National Astronomical Observatories, Chinese Academy of Sciences, Beijing, China

³Joint institute for VLBI in Europe, P.O. Box 2, 7990 AA Dwingeloo, The Netherlands

⁴Institute of Space and Astronautical Science, Yoshinodai 3-1-1, Sagamihara, Kanagawa 229-8510, Japan

optical magnitude, and has been detected at the near infrared K band (Lebofsky et al. 1983). The source shows a flat spectrum between 178 MHz and 37 GHz with the spectral index $\alpha = -0.34$ ($S_\nu \propto \nu^\alpha$). At the VLA angular scale, the source extends to about $1''$ in the northern direction with a very weak polarization indicative of the magnetic field parallel to the jet structure (Perley 1982; O’Dea et al. 1988).

The quasar J1625+4134 has been observed with VLBI at various frequencies: 1.67 GHz (Polatidis et al. 1995), 2.32 and 8.55 GHz (Fey & Charlot 1997); 5 GHz (Pearson & Readhead 1988; Fomalont et al. 2000; Lister et al. 2001a). On the VLBI scale, its structure is rather uncommon: a short strong jet towards the southwest and a long but weak jet emission extended to the north–northwest. The VLBI images at 1.67 and 2.32 GHz are similar, the jet of J1625+4134 extends to the north to over 30 mas along the same position angle $PA = 350^\circ$ as that in the VLA images. Model fitting of the VLBI data revealed a component in the southwest region which was not clearly separated from the central compact emission in the images probably due to the limited angular resolution (Polatidis et al. 1995; Fey & Charlot 1997). The VLBI images at 5 and 8.55 GHz showed a compact core, a short curved jet in the southwest region and a weak emission to the north. The high resolution VSOP image at 5 GHz showed the structure of the southwest jet only, while the image made with the ground-only array (VLBA) of the same VSOP observation exhibited the two-sided jet structure (Lister et al. 2001a) extending both in southwest and north directions. This kind of sharp difference between VLBI structures at low frequencies (and also lower angular resolutions) and higher frequencies (and higher angular resolutions) is relatively rare in AGNs. Another similar case has been found in the high redshift quasar 1351-017 ($z = 3.707$, Frey et al. 2002).

There are several possible explanations for this morphological difference seen in the jet structure of J1625+4134 at different frequencies and angular scales. It has been found that milliarcsecond-scale jets in many radio loud sources is misaligned with respect to the structure at the arcsecond scale (Pearson & Readhead 1988; Hong et al. 1998; Cao 2000). The large ΔPA (the difference between the jet position angles measured on mas and arcsecond scales) may be due to the projection of a bending jet or a helical jet (Conway & Murphy 1993). If the brightest component in the images is the VLBI jet base, J1625+4134 can be classified as a quasar with a sharp bend. For the jet moving away from the core toward the northern emission, ΔPA is about 90° (Lister et al. 2001b) or 270° depending on the jet bending direction.

Alternatively, the brightest component in the 5 and 8.5 GHz images could be not the core of J1625+4134. Rather, the core could be weak and located, e.g., at the end of the southwest emission. In this case the brightest emission in the 5 and 8.5 GHz images may be

caused by interaction of the jet with the ambient medium. The jet turns for about 90° to the north in this region of strong jet-medium interaction. Such the interaction will produce a strong shock, which further enhances the emission and flattens the spectrum.

The third possibility is that the source has a twin-jet structure with the radio jet lying close to the sky plane. In this case, the relativistic boosting effect is not important, the jet and counter-jet are both detectable. The jet emission should be more symmetric at the higher frequencies due to the reduced free-free absorption of the obscuring accretion disk or torus.

In this paper we present and discuss the results of VLBA observations at 22 and 15 GHz. In Section 2, we describe the observations and data reduction. The results are presented in Section 3. In Section 4, we discuss the jet morphology. Throughout this paper we adopt the Hubble constant $H_0 = 65 \text{ km s}^{-1} \text{ Mpc}^{-1}$ and the deceleration parameter $q_0 = 0.5$, assuming the cosmological constant $\Lambda = 0$. With these parameters, 1 milliarcsecond (mas) corresponds to 5.91 pc at the redshift of $z = 2.55$.

2. OBSERVATIONS AND DATA REDUCTION

The observations of J1625+4134 at 22 GHz were conducted with the VLBA on 1 March 2000, the total on-source time was about 3 hours. The LCP signals were recorded in 4 IF-bands for a total bandwidth of 32 MHz with 2-bit sampling. Two strong calibrators, J1635+3805 and J1640+3946, were observed too. The data were then correlated at the VLBA correlator in Socorro (NM, USA) and calibrated and fringe-fitted using the NRAO Astronomical Image Processing System (AIPS) software. Initial amplitude calibration was carried out with the system temperature measurements and the NRAO-supplied gain curves, before the fringe-fitting, the data are corrected for 2-bit sampling errors and atmospheric opacity. The imaging and self-calibration were carried out in DIFMAP package (Shepherd et al. 1994). The constant gain corrections of the stations during the self-calibration are well in agreement with those for the two calibrators.

The source was also observed as part of the VLBA survey at 15 GHz in support to the VSOP Survey Programme (Gurvits et al. 2002). The observation was conducted on 2 January 1999 with a total bandwidth of 64 MHz using 8 IF-bands and 1-bit sampling; the total on-source time was about 35 minutes (7 scans \times 5 minutes). The data on J1625+4134 were calibrated and fringe-fitted alongside with other survey sources, but for the purpose of this work the image was produced independently using AIPS.

3. RESULTS

3.1. Images

The left panel in Fig. 1 presents the naturally weighted image of J1625+4134 at 22 GHz. The estimated thermal noise (1σ) is about 0.3 mJy/beam for 3 hours on-source integration, the lowest contour in the image is 0.9 mJy/beam. The core-jet morphology is consistent with those observed at 5 and 8.5 GHz, the jet bends smoothly to the southwest from the brightest spot and the emission becomes diffuse at about 3 mas.

The naturally weighted image at 15 GHz is shown in the right panel of Fig. 1. The estimated thermal noise (1σ) is about 0.4 mJy/beam for 35 minutes on-source integration, the lowest contour in the image is 1.0 mJy/beam. The general source structure at this frequency is similar to that at 22 GHz. However, one can notice traces of a weak emission at 15 GHz north-northwest at a distance of about 3 mas from the brightest component coinciding with the northern components seen in the images at 5 and 8.5 GHz (Pearson & Readhead 1988; Lister et al. 2001a; Fey & Charlot 1997).

The 5-component model represents well the core-jet structure at 22 GHz and is listed in Table 1. The calibrated u, v -data at 15 GHz were also fitted by 5 Gaussian components (see Table 1), but there is a very low surface brightness emission in the northern region in the residual map. The estimated flux density of this low brightness emission is about 14 mJy. In order to compare our results with other observations, we follow the labeling convention of the jet components introduced by Lister et al. (2001a) in their 5 GHz VSOP image. The component from our model called C2B and present in both 15 and 22 GHz data (see Fig. 1 and Table 1) is absent in the VSOP image at 5 GHz by Lister et al. (2001a). In Table 1, we also give the error estimations of the flux density and the position of the model components. The flux density errors of the model components include the calibration uncertainty as well as the spread in model-fitting results obtained in AIPS and DIFMAP. The error estimation of the component positions are determined by the differences between different model-fitting procedures and the uncertainties estimated by the formula introduced by Fomalont (1988).

The component D is the strongest and the most compact at both 15 and 22 GHz. It has a flat spectrum at the higher observing frequencies, which, following the existing convention, allows us to identify this component as a 'core'. At the brightness level of 1 mJy/beam, no evidence of the counter-jet emission was found in the opposite direction of the bright jet. The weak emission in the north-northwest region at 15 GHz does not seem to resemble a collimated counter-jet, although such an interpretation cannot be ruled out at this stage.

3.2. The distribution of the VLBI component positions

The right panel in Fig. 2 presents a plot of the position of the jet components measured at different frequencies in the quasar J1625+4134 relative to the core component D. The two-sided jet structure consists of a short bright jet bending from the west to the southwest at a few mas from the core and a long weak jet extending to the north for more than 25 mas. If the curved southwest jet continuously bends to the north, the overall bending is at least $\Delta\text{PA} \approx 270^\circ$. Such an extreme bending on the VLBI scale is relatively rare in the known radio structures in AGNs.

The left panel of Fig. 2 shows the enlarged southwest jet. Within the inner 2 mas from the core, the jet components at 8, 15 and 22 GHz follow the same trajectory moving away from the core. But there is about 15° difference in jet axis position angle between the observations at these higher frequencies and the VSOP result at 5 GHz (Lister et al. 2001a).

A careful inspection of our model-fitting results by allowing the change in PA shows that the uncertainties in the determination of the position angle for the inner 2 mas components are less than a few degrees. We also note that our model fitting results at 15 and 22 GHz are in good agreement with those at 8 GHz (Fey & Charlot 1997). All this indicates that the offset of the jet axis at 5 GHz and higher frequencies is real.

Frequency-dependent offsets in the position of jet axis at the VLBI scale have been seen in 3C 454.3 at frequencies 15 and 86 GHz (Krichbaum et al. 1999) and could be caused by the opacity effects enhanced in the regions of stronger jet bending. If the spectral index of the emission region in the transversal direction of the jet is different, the position of the fitted component may shift transversally with the observing frequency. Alternatively, a frequency-dependent core position offset may explain this difference (Lobanov 1998). We also note that the restoring beam of the VSOP observation is $1.08 \text{ mas} \times 0.22 \text{ mas}$ at $\text{PA} = 20^\circ$, and the major axis of the beam is oriented along the offset direction of the jet axis. This alignment could introduce the apparent offset.

In addition to the 22 and 15 GHz VLBA data sets described above, we have got an access to the 5 GHz VLBA data from the VLBApls observations (Fomalont et al. 2000). The image of J1625+4134 from VLBApls was originally model-fitted with two components (Fomalont et al. 2000). In order to compare the models at 5 GHz and higher frequencies, we fitted the self-calibrated VLBApls u, v -data with a 5-component model which includes the northern component B1 detected in both images at 2.3 and 8.5 GHz (Fey & Charlot 1997). The new model-fitting results are given in Table 1. Fig. 3 shows the new model-fitting image based on the VLBIpls data which is consistent with the image published by Fomalont et al. (Fomalont et al. 2000). The positions of the five model components for the VLBApls 5 GHz

data are also shown in Fig. 2. Since the resolution at 5 GHz is lower than that at high frequencies and the structure of the original image at low resolution is simple, the reduced χ^2 of this model-fitting result (for 30 seconds averaged data) is relatively high, 2.29. The new model result cannot be considered as unique, it represents only one of many possible fits.

3.3. Variations of VLBI structure

The C2 component is present in the VLBI models at 5 (both VSOP and VLBApl observations), 8, 15 and 22 GHz. It is located at the same position angle (about -110°) in all observations except the VSOP one. In the latter, the component C2 is some 15° off the position in all other data sets. If the C2 component in all the observations indeed corresponds to the same physical component, its apparent proper motion is $\mu = 0.11 \pm 0.04$ mas/yr, corresponding to a $(7.4 \pm 2.7)c$ apparent transverse velocity. The position of component C2 as a function of time and the best fit of its apparent proper motion is shown in Fig. 4. The estimate of proper motion should be treated with caution due to possible opacity effects and spectral variations across the emission region.

3.4. Spectra of the components

VLBI data on the source J1625+4134 mentioned above have been obtained at different epochs (2.3 and 8.5 GHz – at 1995.77; 5 GHz – 1996.42 and 1998.1; 15 GHz – 1999.0; 22 GHz – 2000.16). The UMRAO monitoring program at 4.8, 8.0 and 14.5 GHz shows that the total flux density of the source varied for up to 30% during the period 1995–2000. In spite of the source’s variability and non-simultaneous VLBI data at different frequencies we attempted to compose and analyze the spectra of the components. The spectra are shown in Fig. 5. Although these spectra are no more than very rough estimates, they offer some useful insight into the radio emission from the jet components.

The component D has a flat spectrum with $\alpha = 0.15 \pm 0.26$ between 5 and 22 GHz. The higher flux density at 2.3 GHz may be due to the lower resolution which may allow for a contribution from low brightness extended emission surrounding the source. Based on its spectrum, the component D is the most likely candidate for the ‘core’ of the source.

The components C2, C2B and B1 have steep spectra. The spectral index of the component C between 5 and 22 GHz is $\alpha = -1.3 \pm 0.3$ (the VSOP data is not included in this spectral index estimate). The component C2B has $\alpha = -1.2 \pm 0.3$ between 8 and 22 GHz,

its turnover frequency is probably between 5 and 8 GHz. The northern component B1 shows similar spectrum with the component C2B, $\alpha = -1.1 \pm 0.3$ between 2 and 15 GHz.

To obtain a two-frequency non-simultaneous spectral index map of the area around the core of J1625+4134, we produced the images at 15 and 22 GHz using the same u, v -ranges, cell size and restoring beams. The problem of producing a spectral index map is in determining the reference position in two images. We have decided to use the position of peak emission of the core component D to align the two images. An eastward shift of 0.04 mas (0.6 pixels) in right ascension was needed in the image at 22 GHz to align its D component with its counterpart at 15 GHz. We note that due to the possible self-absorption in the core region, the peaks of emission may lie in different parts of the core at different frequencies. However, the frequency difference between 15 and 22 GHz is relatively small. If the absolute core position is $r \propto \nu^{-1}$ (Lobanov 1998), the estimated frequency-dependent position difference of the core in J1625+4134 is < 0.1 mas. Fig. 6 shows the spectral index distribution superimposed with the contours of the 15 GHz image.

As one would expect, in spite of an unknown impact of the source variability, the core area of the source has a flat spectrum. The jet region has mostly steeper spectrum, with two noticeable exceptions associated with the component C2 and the area between the components C2B and C1. The flatter spectrum around component C2 is likely to reflect the motion of the component outwards: the leading edge of the component is brighter at higher frequencies resulting in the flatter overall component spectrum. The second region of a flatter spectrum between the components C2B and C1 might be related to the structure variation or to the true spectral index distribution as well as the structural change as in the case of the component C2.

3.5. The brightness temperature of the mas-scale jet components

The brightness temperature T_b of an elliptic Gaussian component in the source rest frame is given by (Shen et al. 1997)

$$T_b = 1.22 \times 10^{12} (1 + z) \frac{S_\nu}{\nu_{ob}^2 ab}, \quad (1)$$

where S_ν is the flux density of the component in Jy at the observing frequency ν in GHz, a and b are the major and minor axes in mas respectively, and z is the source redshift. The brightness temperature distribution of the VLBI jet components, measured at the different frequencies, is shown in Fig. 7. Due to the resolution limit, the brightness temperature

of the core may be only a lower limit and the source variation also may introduce some uncertainties in the estimate of the brightness temperatures.

The brightness temperature of the core is plotted in both panels of Fig. 7. The high brightness temperature of the component D also supports its identification as the core. The brightness temperature decreases sharply within about 4 mas from the core in the southwest region. However, the brightness temperature in the northern jet is relatively constant from 4 to 25 mas. The decrease of the brightness temperature in the inner jet may be due to radiation losses and bending of the jet. If the brightness temperature variations are dominated by the variation of the viewing angle, the jet bending reduces the Doppler boosting effect in the southwest jet, while the orientation of the jet remains relatively unchanged in the northern region.

4. Discussion

4.1. Spectral energy distribution of J1625+4134

Using the data available in NED, we estimated the source rest-frame spectral energy distribution (SED). An upper limit flux density of $0.85 \mu\text{Jy}$ at 1 keV was measured by HEAO-A1 (Biermann et al. 1987). In the ROSAT-FIRST correlation study, Brinkmann et al.(2000) found 5 radio sources within the resolution of ROSAT around J1625+4134. Of these five, J1625+4134 is the nearest one to the ROSAT pointing center (the position offset is $5''$). The X-ray flux measured by ROSAT from this area is $0.14 \pm 0.05 \times 10^{-12} \text{ erg s}^{-1} \text{ cm}^{-2}$. The information on the photon index for this source is unavailable, thus we have used the mean value of 2.46 for the quasars (Brinkmann et al. 2000). This leads to the estimated flux density of $0.012 \mu\text{Jy}$ at 1 keV.

The peak frequency of the synchrotron emission energy, $\nu_{\text{peak}} = 3.4 \times 10^{12} \text{ Hz}$, is located in the sub-mm band, the spectral energy at the peak frequency, $\nu L_\nu = 8.8 \times 10^{38} \text{ W}$, is typical for the radio-loud quasars (Sambruna et al. 1996). The X-ray emission could not fit the synchrotron emission, most likely this is to be attributed to the Self-Synchrotron Compton scattering (SSC).

4.2. Doppler boosting

J1625+4134 is a typical radio loud quasar which shows all the indications on the relativistic bulk motion of the plasma in its jet, with its synchrotron emission Doppler boosted.

There are several methods of estimating the Doppler boosting factor.

Assuming that the X-ray emission mechanism is SSC scattering, one can adopt the equation (1) of Ghisellini et al. (1993) to estimate the Doppler boosting factor δ_{sp} in a uniform sphere of the emission region. Readhead (1994) suggested another method of estimating the Doppler boosting factor, the so called equipartition Doppler boosting factor δ_{eq} . The method is based on the assumption on the energy equipartition between the radiating particles and the magnetic field.

Both methods above require VLBI core data at the turnover frequency. It proved to be difficult since the core has a very flat spectrum (see Fig. 5). In Table 2, we list the Doppler boosting factor estimates using both methods by assuming VLBI observing frequencies as the VLBI core turnover frequency. To avoid a fitted zero axial ratio for the 8.5 GHz core (Fey & Charlot 1997), we used a value of 0.2 for this ratio in the calculation.

In the equipartition case, a correction of the core size, $\theta_d = 1.8\sqrt{ab}$ was applied (Marcher 1987; Güijosa and Daly 1996), while in the δ_{sp} estimate, a factor of 0.8 was adopted (Güijosa and Daly 1996). The new X-ray flux density was used in the δ_{sp} estimate and the spectral index $\alpha = -0.75$ for the optically thin synchrotron emission was assumed. Table 2 gives the estimates of the Doppler boosting factor for VLBI core data obtained at different frequencies.

Jiang et al. (1998) investigated the inhomogeneous jet parameters in the Königl’s model (Königl 1981). In this model, a VLBI core is believed to be a base of the optically thick synchrotron emission region of an inhomogeneous jet. Assuming that the X-ray emission mechanism is the SSC scattering and the distributions of the magnetic field and the relativistic electron number density in the jet follow the power law ($m = 1$ for the magnetic field and $n = 2$ for the electron number density), and using the value of the proper motion of $\mu = 0.11$ mas/yr, we can obtain the Doppler boosting factor and estimate other parameters of the model. The Doppler boosting factors δ_{jet} for the inhomogeneous jet model are also given in Table 2.

These estimates of the Doppler boosting factor values cover a wide range of VLBI core parameters obtained at different frequencies. We assume the mean value $\delta = 5.2 \pm 2.5$ as the best estimate of the Doppler boosting factor in the jet of J1625+4134. Combined with the proper motion mentioned above, the viewing angle to the line of sight could be estimated as $\theta = 10^\circ \pm 4^\circ$, and the Lorentz factor of the jet $\gamma = 8 \pm 4$. These parameters are consistent with those for radio-loud quasars.

4.3. Possible explanation for the jet structure

The proper motion, non-detection of the counter-jet and the estimated value of the Doppler boosting factor suggest that the orientation of the inner south-west jet is close to the line of sight. These arguments rule out a two-sided jet morphology as an explanation of the observed bi-directional (southwest and north-northwest) jet structure in J1625+4134.

In radio-loud AGNs, large apparent bending angles of jet can be explained by the projection effect, since the viewing angle to the line of sight is small. The observed difference in the position angle of different areas along the jet, ΔPA , is related to the true bending angle of the jet $\Delta\phi$ as

$$\cos\Delta\phi = \cos\theta_1\cos\theta_2 + \sin\theta_1\sin\theta_2\cos\Delta PA, \quad (2)$$

where θ_1 and θ_2 are the viewing angles of the jet. The equation (2) holds only for the step change of the $\Delta\phi$. For a curved jet, the accumulated true bending angle $\Delta\phi$ should be integrated along the trajectory of the bending using the small angle approximation. If the jet moves along a cone with the half-opening angle θ_1 (this means that θ_2 is equal to θ_1), the integrated true bending angle $\Delta\phi = \sin\theta_1(\Delta PA)$. In the J1625+4134 case, the estimated viewing angle of the southwest inner jet θ_1 is about 10° . If the two-sided jet is connected via an invisible curved trajectory, $\Delta PA = 270^\circ$ corresponds to $\Delta\phi = 47^\circ$. This is a large intrinsic bending.

The cause for such a large bending of the jet in J1625+4134 is not clear. There is no obvious evidence of the enhanced emission at the region of sharp bending region of its jet. It seems that the bending of the jet is not caused by the interaction with the surrounding medium, since such interaction will produce strong shocks, further enhancing the radio emission.

Another possible explanation for the bi-directional jet structure is the intrinsic change in the jet ejection angle caused by a ballistic precession or erratic change in the nozzle direction. The bi-directional jet structure in J1625+4134 is more like the erratic change in the nozzle direction, because two jets follow two very different ballistic trajectories (Gómez et al. 1990). The northern jet may have been ejected when the nozzle of the jet pointed to the north and the southwest jet is the result of a newer ejection. In this case, the change of the nozzle direction would occur more than about 50 years ago – the time needed for the bending southwest jet material to reach its present extension of about 4-5 mas with the apparent proper motion of the component C2 of about 0.1 mas/yr.

Since the northern emission has a steep spectrum, a high resolution observations with

a higher sensitivity at low frequencies may be useful to distinguish between the two possible models. A detection of the connection between the two jets will support the projection effect explanation.

5. SUMMARY

The quasar J1625+4134 shows an uncommon bi-directional jet structure on the VLBI scale at various observing frequencies. We presented the images of VLBA observations at 15 and 22 GHz, showing a short curved southwest jet which extends for several mas from the core. Our VLBI results, combined with the data available in the literature, allow us to estimate the spectral index of the components and to identify the component D as the VLBI core based on its flat spectrum between 5 and 22 GHz. The jet components distribution at different observing frequencies favors a large difference of about 270° in the position angles of the direction of the jet propagation in the southwest and northern areas from the core. A proper motion of the component C2 in the southwest jet, $\mu = 0.11$ mas/yr, was estimated. Using the multi-band VLBI data on the component D and different physical methods, we obtained the best estimate of the Doppler boosting factor, $\delta = 5.2 \pm 2.5$, corresponding to the southwest inner jet viewing angle of $10^\circ \pm 4^\circ$ to the line of sight with the Lorentz factor $\gamma = 8 \pm 4$.

The proper motion, the estimated Doppler boosting factor and non-detection of the counter-jet emission at the higher VLBI frequencies rule out the two-sided-jet explanation for the observed bi-directional jet morphology. According to the analysis on the relativistic jet parameter, we point out on the possibility that the southwest jet goes to the north via a helical trajectory, while an erratic change in the nozzle direction also can explain the bi-directional jet structure. High resolution VLBI observations at lower frequencies may provide clue on this model.

We found a difference of about 15° in the southwest jet axis between the 5 GHz VSOP image and other VLBA observations at higher frequencies. Our re-analysis of the 5 GHz VLBApl data narrows the difference in the axis position, but the hypothesis on a frequency dependent position of the jet axis needs further verification.

Support from the Chinese fund NKBRFSF (No. G1999075403) is gratefully acknowledged. The VLBA is operated by the National Radio Astronomy Observatory which is managed by Associated Universities, Inc., under cooperative agreement with the National Science Foundation. This paper has made use of the NASA/IPAC Extragalactic Database (NED), which is operated by the Jet Propulsion Laboratory, California Institute of Tech-

nology, under contract with the National Aeronautics and Space Administration. We have also used the data from the University of Michigan Radio Astronomy Observatory which is supported by the National Science Foundation and by funds from the University of Michigan. We are grateful to the teams of VLBApIs (Fomalont et al. 2000) and VLBA 2 cm VSOP support survey (Gurvits et al. 2002) for the permission to re-analyze their data. The authors acknowledge support from the exchange programme in radio astronomy of the Chinese and Dutch Academies of Sciences. We wish also to thank the anonymous referee for the valuable comments.

REFERENCES

- Biermann, P. I., Kühr, H., Snyder, W. A., & Zensus, J. A., 1987, *A&A*, 185, 9
- Brinkmann, W., Laurent-Muehleisen, S. A. Voges, W., Siebert, J., et al., 2000, *A&A*, 356, 445
- Cao Xinwu, 2000, *A&A*, 355, 44
- Conway, J. E. & Murphy, D. W., 1993, *ApJ*, 411, 89
- Fey, A. L. & Charlot, P., 1997, *ApJS*, 111, 95
- Frey, S., et al., 2002, in preparation
- Fomalont, E. B., Frey, S., Paragi, Z., et al., 2000, *ApJS*, 131, 95
- Fomalont, E. B., 1988, in *Synthesis Imaging in Radio Astronomy*, edited by R. A. Perley, F. R. Schwab and A. H. Bridle, 213
- Ghisellini, G, Padovani, P, Celloti, A., 1993, *ApJ*, 407, 65
- Gómez, J., Marscher, A. P., Alberdi, A., and Gabuzda, D. C., 1999, *ApJ*, 519, 642
- Güijosa, A. & Daly, R. A., 1996, *ApJ*, 461, 600
- Gurvits, L.I., Kellermann, K.I., Fomalont, E.B. and Zhang, H.Y., 2002, in preparation
- Hewitt, A., & Burbidge, G., 1993, *ApJS*, 87, 451
- Hong, X. Y., Jiang, D. R. and Shen, Z. Q., 1998, *A&A*, 330, L45
- Jiang, D. R., Cao, X. and Hong, X., 1998, *ApJ*, 494, 139

- Königl, A., 1981, *ApJ*, 243, 700
- Krichbaum, T. P. et al., 1999, in 2nd Millimeter-VLBI Science Workshop, held at IRAM Granada, Spain, 27-29, eds. A. Greve and T. P. Krichbaum, 5
- Lebofsky, M. J., Rieke, G. H. and Walsh, D., 1983 *MNRAS*, 203, 727
- Lister, M. L., Tingay, S. J., Preston, R. A., 2001a, *ApJ*, 554, 948
- Lister, M. L., Tingay, S. J., Preston, R. A., 2001b, *ApJ*, 554, 964
- Lobanov, A. P., 1998, *A&A*, 330, 79
- Marcher, A. P., 1987, in *Superluminal Radio Sources*, eds by Zensus J. A. and Pearson, T. J., Cambridge University Press, New York, 280
- O’Dea, C. P., Barvainis, R., Challis, P. M., 1988, *AJ*, 96, 435
- Pearson, T. J. and Readhead, A. C. S., 1988, *ApJ*, 328, 114
- Perley, R. A., 1982, *AJ*, 87, 859
- Polatidis, A. G., Wilkinson, P. N. et al., 1995, *ApJS*, 98, 1
- Readhead, A. C. S., 1994, *ApJ*, 426, 51
- Sambruna, R. M., Maraschi, L., Urry, C. M., 1996, *ApJ*, 463, 444
- Shen, Z.-Q., Wan, T. S., Moran, J. M., Jauncey, D. L., et al., 1997, *AJ*, 114, 1999
- Shepherd, M. C., Pearson, T. J., & Taylor, G. B., 1994, *BAAS*, 26, 987

Table 1. Gaussian Models

component	s (mJy)	r (mas)	θ (deg)	a (mas)	b/a	ϕ (deg)	χ^2_ν
<u>$\nu = 22$ GHz</u>							
D	284±28	0	0	0.09	0.52	-58	1.00
C3	35±10	0.39±0.04	-96±5	0.48	0.42	70	
C2	60±15	1.30±0.04	-109±3	0.74	0.56	-26	
C2B	34±15	2.06±0.10	-108±4	0.97	1.0	0	
C1	35±20	3.07±1.00	-140±6	2.25	1.0	0	
<u>$\nu = 15$ GHz</u>							
D	273±28	0	0	0.22	0.61	70	1.47
C3	17±13	0.57±0.30	-101±5	0.36	0.00	-44	
C2	80±10	1.13±0.06	-111±3	0.71	0.71	-11	
C2B	82±12	1.936±0.14	-109±4	1.36	1.0	0	
C1	34±12	3.61±0.33	-142±6	1.88	1.0	0	
<u>$\nu = 5$ GHz</u>							
D	342±50	0	0	0.35	1.0	0	2.29
C2	367±50	0.95±0.10	-120±6	0.70	1.0	0	
C2B	173±30	2.33±0.17	-116±6	1.30	1.0	0	
C1	088±30	3.51±1.00	-150±10	2.02	1.0	0	
B1	053±40	3.11±1.10	-44±10	3.34	1.0	0	

Note. — Col.(1) Component name; col.(2) Flux density in Jy Col.(3) Distance from core in mas; Col.(4) Position angle with respect to the core; Col.(5) Major axis of the fitted component in mas; Col.(6) Axis ratio of the fitted component; Col.(7) Position angle of the component’s major axis; Col.(8) Reduced χ^2 of the fit.

Table 2. Doppler boosting factors

VLBI data	22.22 (GHz) this work	15.33 (GHz) this work	8.55 (GHz) FC	5.0 (GHz) this work	2.3 (GHz) FC	1.6 (GHz) PW
δ_{sp}	9.8	3.0	9.2	5.5	6.6	9.1
δ_{eq}	3.5	0.7	4.5	2.5	3.3	5.7
δ_{jet}	5.0	2.3	6.0	4.5	5.3	7.1

Note. — The reference of VLBI core data: FC (Fey & Charlot 1997); PW (Polatidis et al. 1995)

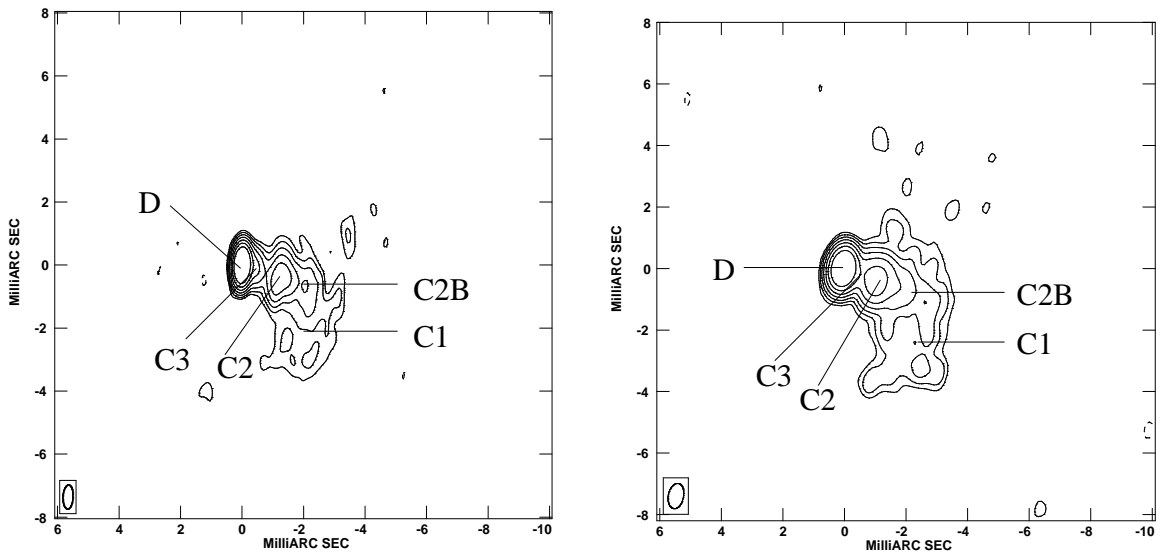


Fig. 1.— Left: the naturally weighted image of J1625+4134 at 22 GHz, the restoring beam is 0.77×0.33 mas at $PA=-2.^\circ 8$, the contour levels are $(-1, 1, 2, 4, 8, 16, 32, 64) \times 0.9$ mJy/beam, the peak flux density is 0.282 Jy/beam. Right: the naturally weighted image of J1625+4134 at 15 GHz, the restoring beam is 0.83×0.50 mas at $PA=-11.^\circ$, the contour levels are $(-1, 1, 2, 4, 8, 16, 32, 64) \times 1$ mJy/beam, the peak flux density is 0.246 Jy/beam.

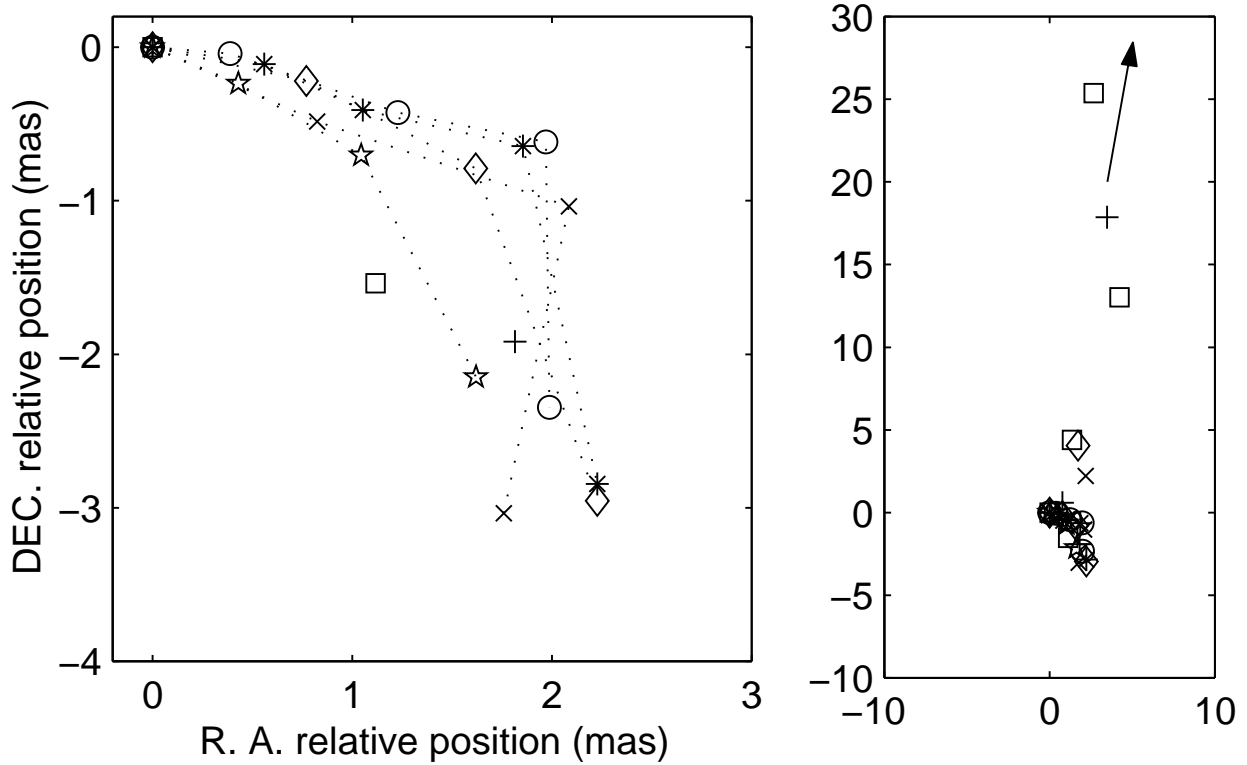


Fig. 2.— The position of all jet components observed in J1625+4134 at various frequencies: 22 GHz (circles, epoch 2000 Mar 1, this work), 15 GHz (asterisks, epoch 1999 Jan 2, this work), 8.5 GHz (diamonds, epoch 1995 Oct 12, Fey & Charlot 1997), 5 GHz (crosses, epoch 1996 Jun 6, this work and Fomalont et al. 2000), VSOP 5 GHz (stars, epoch 1998 Feb 7, Lister et al. 2001a), 2.3 GHz (squares, epoch 1995 Oct 12, Fey & Charlot 1997) and 1.6 GHz (plus, epoch 1990 Sep 21, Polatidis et al. 1995). The arrow indicates the position angle of the emission at the arcsecond scale in the VLA images (O’Dea et al, 1988, Perley 1982).

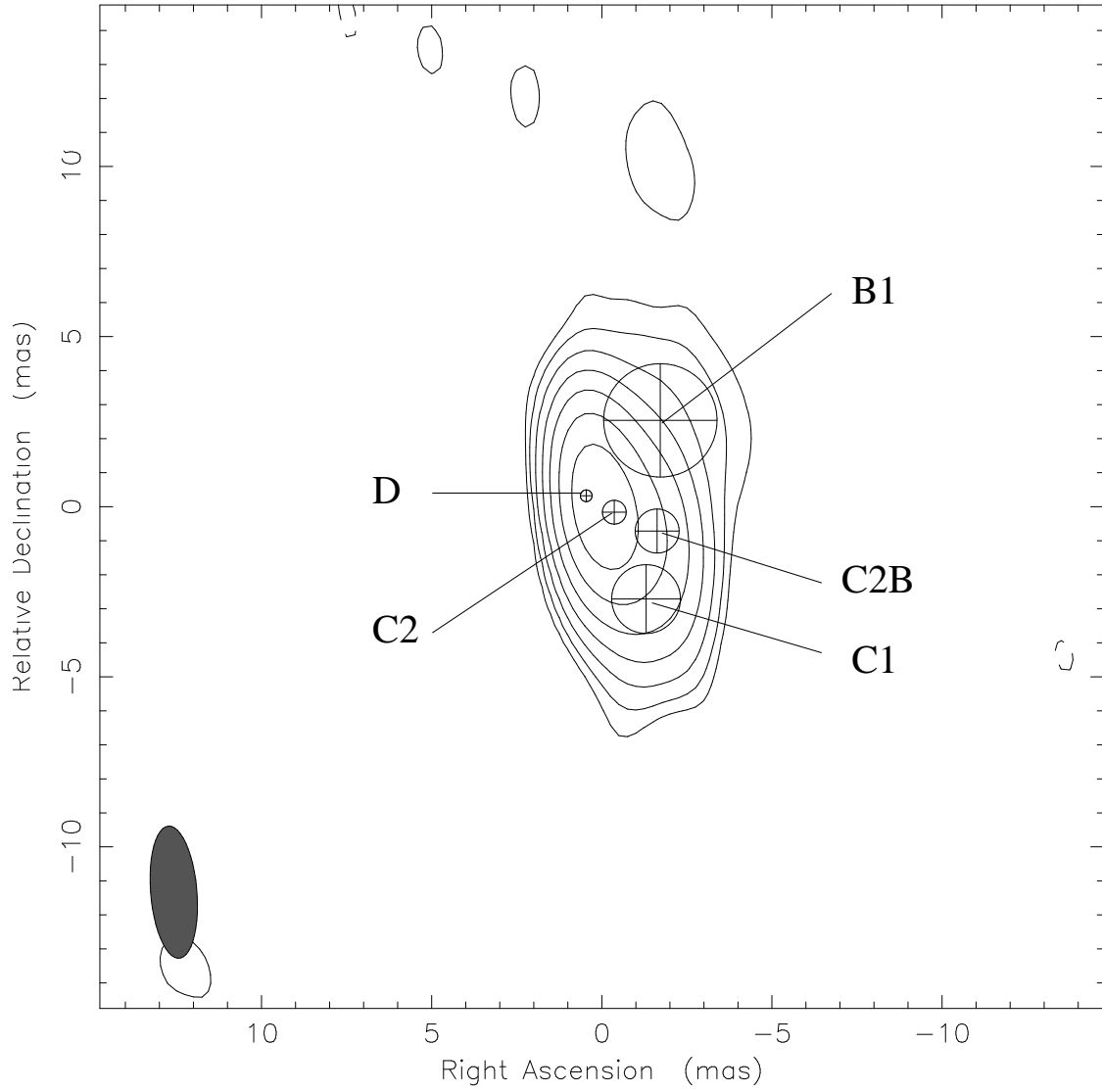


Fig. 3.— The model fitting image of J1625+4134 based on the 5 GHz VLBApls data set (Fomalont et al. 2000). The restoring beam is 3.9×1.36 mas at $PA=4.7^\circ$, the contour levels are $(-1, 1, 2, 4, 8, 16, 32, 64) \times 5$ mJy/beam, the peak flux density is 0.556 Jy/beam.

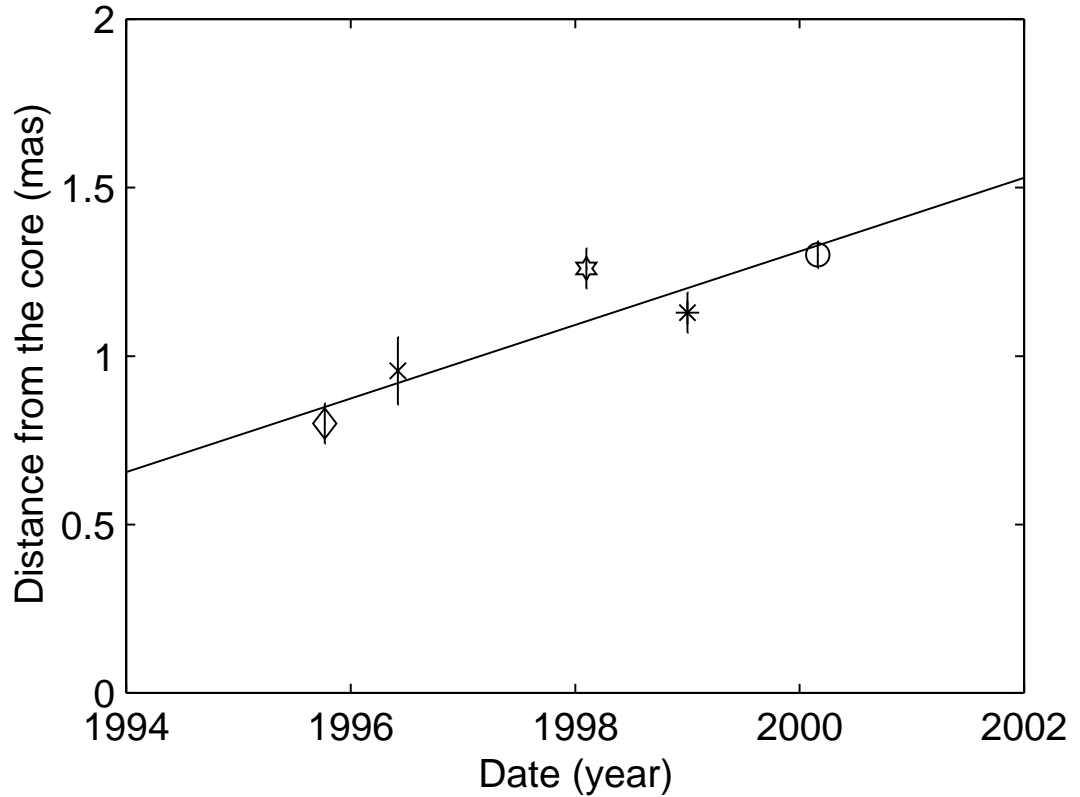


Fig. 4.— Apparent proper motion of the jet component C2 in J1625+4134: 22 GHz (circle, epoch 2000 Mar 1, this work), 15 GHz (asterisk, epoch 1999 Jan 2, this work), 8 GHz (diamond, epoch 1995 Oct 12, Fey & Charlot 1997), 5 GHz (cross, epoch 1996 Jun 6, this work and Fomalont et al. 2000) and VSOP 5 GHz (star, epoch 1998 Feb 7, Lister et al. 2001a). The position errors of the C2 component at 15 GHz, 22 GHz and 5 GHz are in the table 1, and for the errors of the C2 component at 8 GHz and VSOP 5 GHz, a value 0.06 mas is assumed.

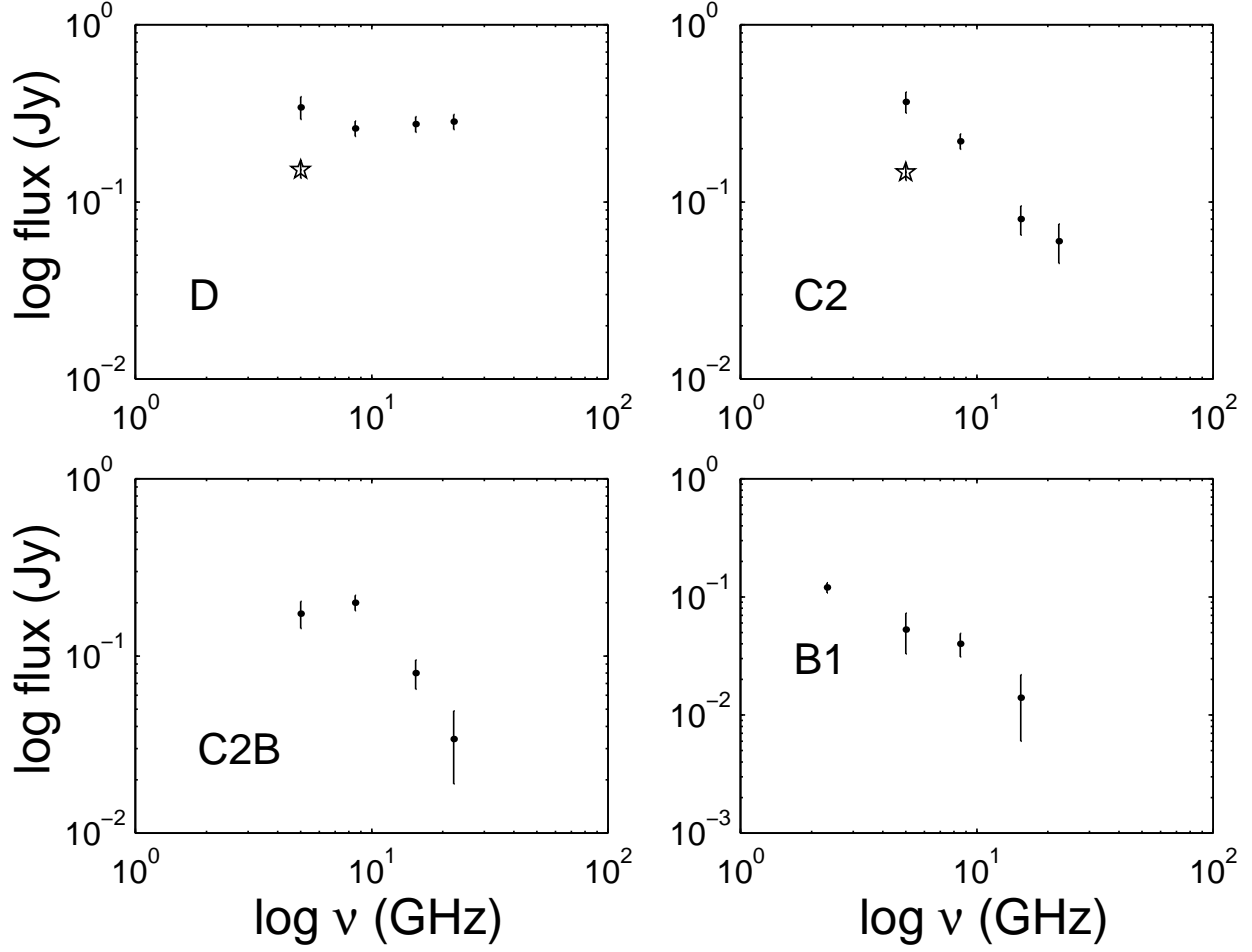


Fig. 5.— Spectra of the jet components in J1625+4134. The stars present the flux density values of the components from VSOP 5 GHz observation. The error estimates of the flux density of the components at 15 GHz, 22 GHz and 5 GHz are in the table 1, and a 10 percent of the flux density for the components at 8 GHz and VSOP 5 GHz are assumed as the estimates of the errors.

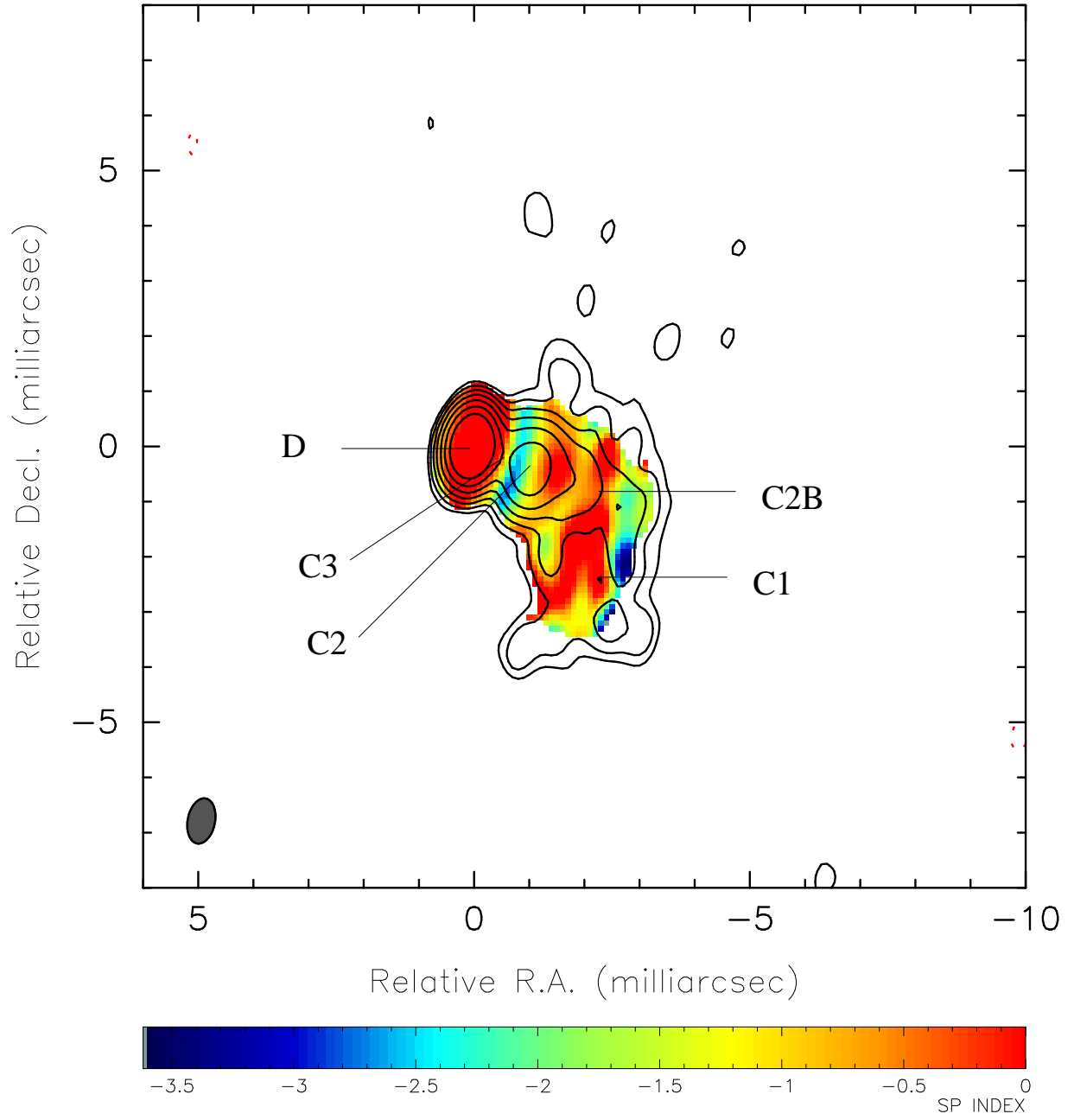


Fig. 6.— The non-simultaneous two-frequency spectral index distribution between 15 and 22 GHz. The wedge at the bottom shows the spectral index scale. The contours are from the 15 GHz image (Fig. 1)

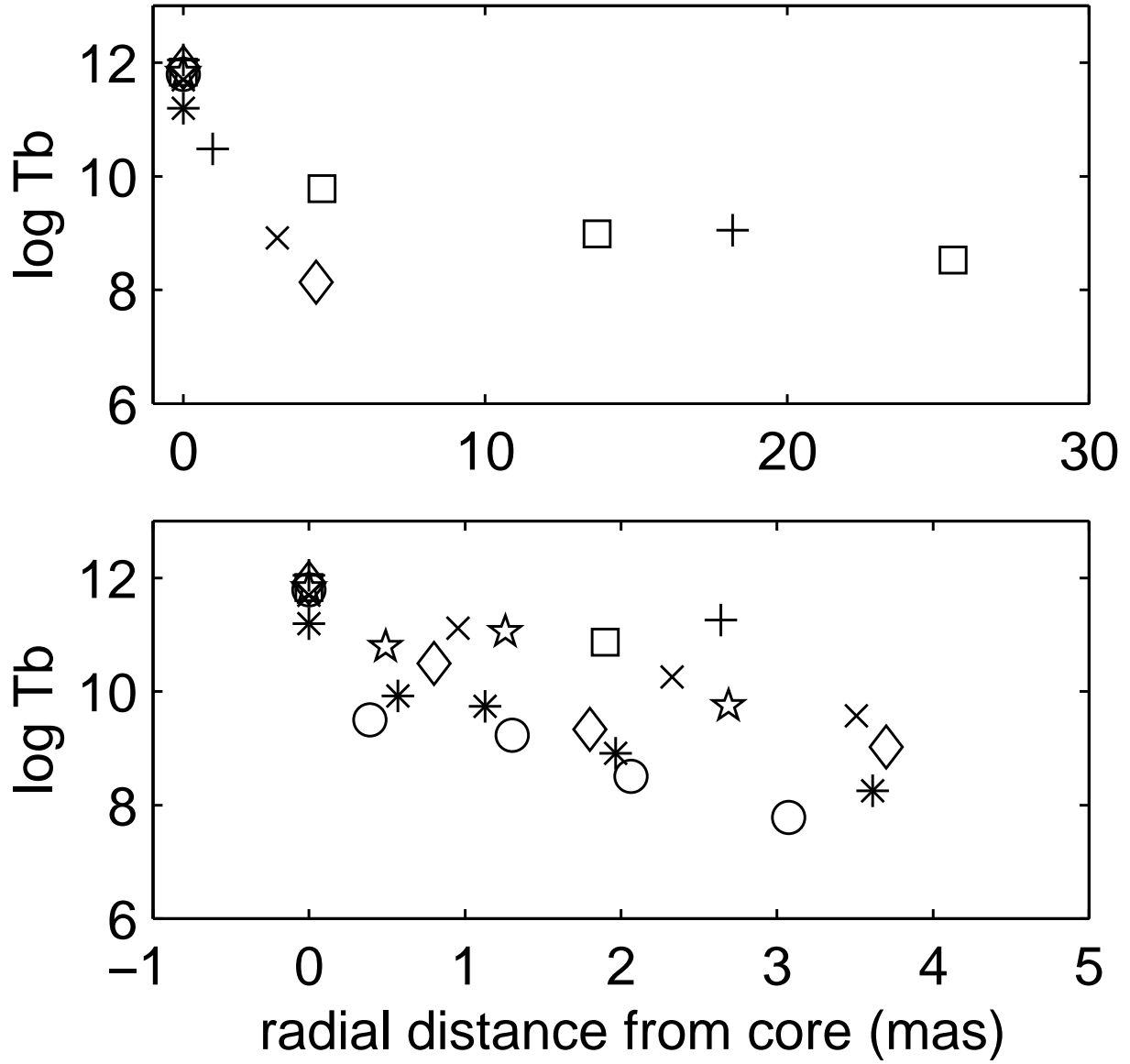


Fig. 7.— The source rest-frame brightness temperature distribution of the VLBI components in the jet of J1625+4134. The upper panel shows the northern jet, the lower panel shows the southwest (inner). The symbols are the same as in Fig. 2.